Estimating $ZZ \rightarrow ll\nu\nu$ background in the $ll + E_T^{miss}$ final state using $Z\gamma \rightarrow ll\gamma$ data

A Thesis

submitted to
Indian Institue of Science Education and Research, Pune
in partial fulfillment of the requirements for the
BS-MS Dual Degree Programme

by

Mangesh Sonawane

Registration Number: 20121083

Indian Institute of Science Education and Research, Pune
Dr. Homi Bhabha Road,
Pashan, Pune 411008, INDIA

June 2017 - April 2018

Conducted at : DESY
Notkestraße 85,
22607, Hamburg
Germany

Supervisor: Dr. Beate Heinemann

Certificate

This is to certify that this dissertation, entitled "Estimating $ZZ \rightarrow ll\nu\nu$ background in the $ll + E_T^{miss}$ final status using $Z\gamma \rightarrow ll\gamma$ data", submitted towards the partial fulfilment of the BS-MS dual degree programme at the Indian Institute of Science Education and Research (IISER), Pune, represents the work carried out by Mangesh Sonawane at the Deutsches Elektronen-Synchrotron (DESY), Hamburg, under the supervision of Dr. Beate Heinemann, Professor of Experimental Particle Physics at the Institute of Physics, University of Freiburg, during the academic year 2017-2018.

Mangesh Sonawane   Dr. Beate Heinemann

Committee:
Dr. Beate Heinemann
Dr. Seema Sharma

I dedicate this thesis to my parents, Avinash and Ranjana Sonawane, my mentors, Dr. Sourabh Dube and Dr. Seema Sharma, and to my friends and colleagues and IISER, without whose timely advice and support this thesis would not have been made possible.

Declaration

I hereby declare that the matter containined within the thesis entitled "Estimating $ZZ \rightarrow ll\nu\nu$ background in the $ll + E_T^{miss}$ final status using $Z\gamma \rightarrow ll\gamma$ data", contains the results of the work carried out by me at the Deutsches Elektronen-Synchrotron (DESY) Hamburg, under the supervision of Dr. Beate Heinemann, and the same has not been submitted elsewhere for any other degree.

Mangesh Sonawane

Dr. Beate Heinemann

Committee:
Dr. Beate Heinemann
Dr. Seema Sharma

Acknowledgements

I would like to express my deepest gratitude for Dr. Beate Heinemann for her guidance and patient mentoring. It's not just technical skills that I have acquired under her supervision, but also an understanding of how a physicist approaches the subject and tackles the inevitable problems that surface.

⟨ placeholder ⟩

Abstract

In the search for Dark Matter (DM) at the LHC, SM particles are produced in association with DM particles, which are invisible as they don't interact with the detector. Thus events with large imbalance in transverse momentum are of interest. One such signature is $ll + E_T^{miss}$. The dominant background contributing to the search for DM in the $ll + E_T^{miss}$ is $ZZ \rightarrow ll\nu\nu$. Currently, this background is determined using Monte Carlo simulation, with an uncertainty of $\approx 10\%$ [1]. The goal of this study is to establish a data driven method to estimate this background, and reduce the uncertainty. Using $Z\gamma \rightarrow ll\gamma$, which is a process with low backgrounds and has a high $BR{*}\sigma$, it is possible to estimate the $ZZ \rightarrow ll\nu\nu$ contribution. In regions where $p_T(\gamma) \gg M_Z$, the two processes are kinematically similar. They have the same production mechanisms, but differ due to the photon and Z boson couplings to the quarks being different, as well as the difference in mass (photons are massless, while Z bosons are massive). Introducing a transfer factor R as the ratio $\sigma(ZZ)/\sigma(Z\gamma)$ which is determined from simulation, the contribution of $ZZ \rightarrow ll\nu\nu$ to the background can be estimated from $Z\gamma \rightarrow ll\gamma$ data. The uncertainty on the prediction of R due to theoretical aspects is estimated in this work.

Contents

Chapter 1

Introduction

The Standard Model of physics is one of the most successful theories developed, describing the fundamental forces and their interactions. It is theoretically self-consistent, and has enjoyed tremendous success in providing stunningly accurate experimental predictions. However, the Standard Model is not complete theory. It does not provide an explanation for several observed phenomena, such as gravity, or the accelerating expansion of the universe, among others.

One such question that triggers burning curiosity is the apparent incongruity of galaxy rotation curves with the theory of Newtonian mechanics: stars in the arms of spiral galaxies appear to move much faster than Newtonian physics would predict. Either the current understanding of mechanics is incomplete, or there is more mass present somewhere in the galaxy that is not visible by any method that is currently employed. This invisible hunk of matter is what is termed as Dark Matter (DM).

Detailed observations of these rotation curves, along with measurements of other phenomena such as gravitational lensing by distant galaxies, galaxy clusters, and Cosmic Microwave Background (CMB) lead to the conclusion that, if the Dark Matter hypothesis is true, the amount of visible Baryonic matter in the universe is a mere 4%. The remaining 96% of the universe is composed of Dark Matter and Dark Energy.

Now it becomes important to address the question: what exactly is Dark Matter?

Several extensions to the Standard Model, called Beyond Standard Model (BSM) theories, attempt to provide an explanation of these observed phenomena. Dark Matter hasn't been observed to interact directly through the electromagnetic, strong or weak nuclear forces, consequently candidates for Dark Matter are called Weakly Interacting Massive Particles (WIMPs). In LHC experiments, events with WIMPs in the final state show up as an imbalance in the momentum in the plane transverse to the beam (referred to as E_T^{miss} throughout this thesis).

One such BSM theory postulates that these Dark Matter candidate particles may couple to Standard Model particles in interactions mediated by the Higgs boson. Fig 1.1 illustrates some of the possible processes for the production of the Higgs boson, where the Higgs boson further decays into invisible particles.

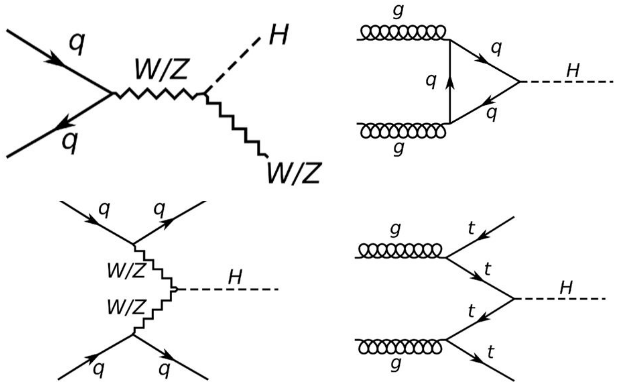

Figure 1.1: Feynman diagrams for the Standard Model production of the Higgs boson; VH: Higgs produced in association with a W/Z boson (top left), ggF: gluon-gluon fusion (top right), VBF: vector boson fusion (bottom left), ttH: (bottom right). The Higgs boson then further decays into invisible DM particles.

In this thesis, a closer look is taken at the VH channel, in particular ZH, where the Higgs boson decays invisibly into DM particles, and the Z boson decays into a dilepton pair. The signature of such a process is $ll + E_T^{miss}$. A Dark Matter search in this channel would be to stack all known Standard Model processes that contribute to the $ll + E_T^{miss}$ signal (these form the background) and look for excesses which will indicate the presence of non Standard Model processes. In this thesis, a closer look is taken at the $ZZ \to ll\nu\nu$ process, which constitutes the dominant SM background in the $ll + E_T^{miss}$ final state. However, it is difficult to discriminate between the Standard Model $ZZ \to ll\nu\nu$ and $ZH \to l^+l^- + E_T^{miss}$, the process under consideration, because of the identical final state. Thus, an attempt s made to estimate it using alternate processes with clean signals.

1.1 The Standard Model

The Standard Model is the name given to the theory of particles, fundamental forces, and interactions that govern the Universe. It describes three of the four forces: the electromagnetic, strong and weak forces. Figure **??** shows a schematic representation of the elementary particles in the Standard Model.

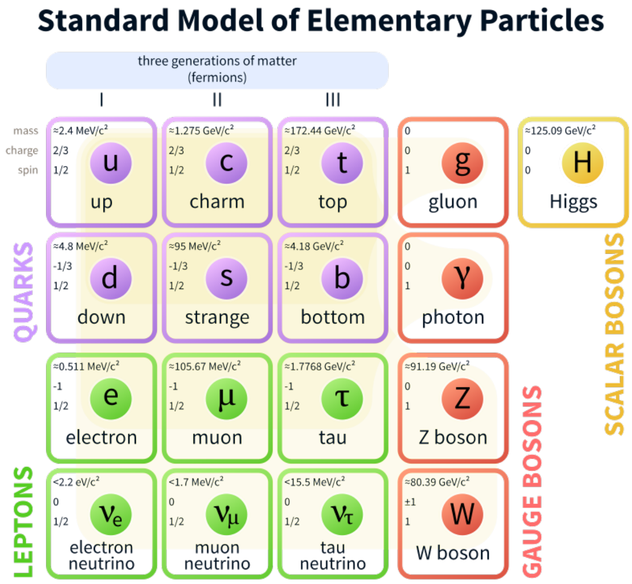

Figure 1.2: A schematic representation of the Standard Model of particles. The table shows the three generations of fermions (classified as quarks and leptons) that are the building blocks of all known matter in the universe, and bosons that mediate interactions, and are thus responsible for 'forces'

1.2 Theoretical tools

Chapter 2

The Large Hadron Collider

Chapter 3

Analysis

3.1 Motivation

Chapter 4

Theoretical uncertainties on cross sections and the transfer factor R

It is worth reiterating that the goal of this thesis is to use $Z\gamma \to ll\gamma$ process to estimate the dominant contribution $ZZ \to ll\nu\nu$ to the Standard Model $ll + E_T^{miss}$ background. Excesses would indicate the presence of BSM physics. It is thus important to have an estimate of the uncertainties on the theoretical predictions of the ZZ and $Z\gamma$ cross sections, and the transfer factor R.
In this study, the following sources of uncertainities are studied.

- Scale Uncertainties: contributions due to higher order QCD corrections cannot be calculated to arbitrarily high order, as it gets progressively more computationally expensive. Thus, this study is limited to Next to Leading Order (NLO), and further corrections are accounted for as scale uncertainties.
- PDF Uncertainties: a proton-proton collision involves the interaction of the composite quarks and gluons (partons) at very high energies. These partons carry a fraction of the proton momentum. Parton Distribution Functions (PDFs) represent this fraction of proton momentum carried by partons as probability distributions. Owing to the non-deterministic nature of this fact, this study attempts to account for this uncertainties as PDF uncertainties.
- Photon Fragmentation Uncertainties: in the $Z\gamma \to ll\gamma$ process, the signal includes a photon. However, while reconstructing the event, soft photons, or photons resulting from other fragmentation processes may be encountered. To ensure that the photon is indeed prompt, it is required to be isolated from hadronic activity (such as pion decays). This isolation is implemented experimentally in different ways. The uncertainty associated with the implementation of this isolation is estimated as photon fragmentation uncertainties.

To characterize these uncertainties, we use a programme, MCFM, to generate cross sections for $ZZ \to ll\nu\nu$ and $Z\gamma \to ll\gamma$ processes, and vary the relevant parameters such as scale, PDF sets, and photon isolation effects to obtain an estimate of the uncertainties.

4.1 MCFM

MCFM is a program that calculates cross sections for femtobarn-level processes at LO or NLO. In this study, MCFM v8.0 [4] is used to produce cross sections of $ZZ \to ll\nu\nu$ and $Z\gamma \to ll\gamma$ processes at NLO, with a selection of generator level cuts. The samples are generated with cuts on $E_T^{miss} = p_T(Z \to \nu\nu)$ for the ZZ process and $E_T^{miss} = p_T(\gamma)$ for the $Z + \gamma$ process. A ratio of these cross sections is taken to obtain the R distribution as a function of p_T. The uncertainty on R is calculated by varying several parameters at the generator level, such as the renormalization and factorization scales, the PDF sets used, photon fragmentation, etc. Effects of applying lepton cuts on the cross sections as well as on the ratio are studied. The contributions of the $q\bar{q}$ and gg processes are estimated separately.

MCFM does not produce $Z \to ll$ but $Z \to ee$. As electrons and muons have similar properties with the exception of mass, simply the branching fraction of $Z \to ee$ must be accounted for to obtain the inclusive value of R.

$$R_{inc} = R * \frac{BR(Z \to ee)}{BR(Z \to ee) * BR(Z \to \nu\nu) * 2} \tag{4.1}$$

4.2 Generator Parameters

The samples are generated using MCFM v8.0 for the following data points:

$$\text{For } ZZ \to ee\nu\nu : E_T^{miss} > \{50, 75, 100, 125, 150, 200, 250, 300, 400, 500\} \text{ GeV}$$
$$\text{For } Z(\to ee) + \gamma : p_T(\gamma) > \{50, 75, 100, 125, 150, 200, 250, 300, 400, 500\} \text{ GeV}$$

Table 4.1 lists the generator level settings used for the ZZ and $Z + \gamma$ processes. All lepton cuts are consistent with the ones used in the ATLAS Z+E_T^{miss} analysis.

Cuts	$ZZ \to ee\nu\nu$	$Z(\to ee) + \gamma$
Process ID	87	300
M_{ee}	$81 < M_{ee} < 101$ GeV	$81 < M_{ee} < 101$ GeV
$M_{\nu\nu}$	-	-
Order	NLO	NLO
PDF set	CT14	CT14
$p_T^{\text{lead}}(e)$	> 30 GeV	> 30 GeV
$\lvert\eta^{lead}(e)\rvert$	< 2.5	< 2.5
$p_T^{\text{sublead}}(e)$	> 20 GeV	> 20 GeV
$\lvert\eta^{sublead}(e)\rvert$	< 2.5	< 2.5
$\Delta R(\gamma, e)$	-	0.7
Renormalization scale	91.187 GeV (M_Z)	91.187 GeV (M_Z)
Factorization scale	91.187 GeV (M_Z)	91.187 GeV (M_Z)

Table 4.1: Settings in input.DAT for MCFM

The constraint on M_{ee} in the case of $Z + \gamma$ suppresses the FSR process by ensuring that the lepton pair are from a Z decay only.

4.3 Results

Using the settings listed in Table 4.1, the cross sections shown in Figure 4.1 are obtained. Throughout this analysis, this sample is the reference.

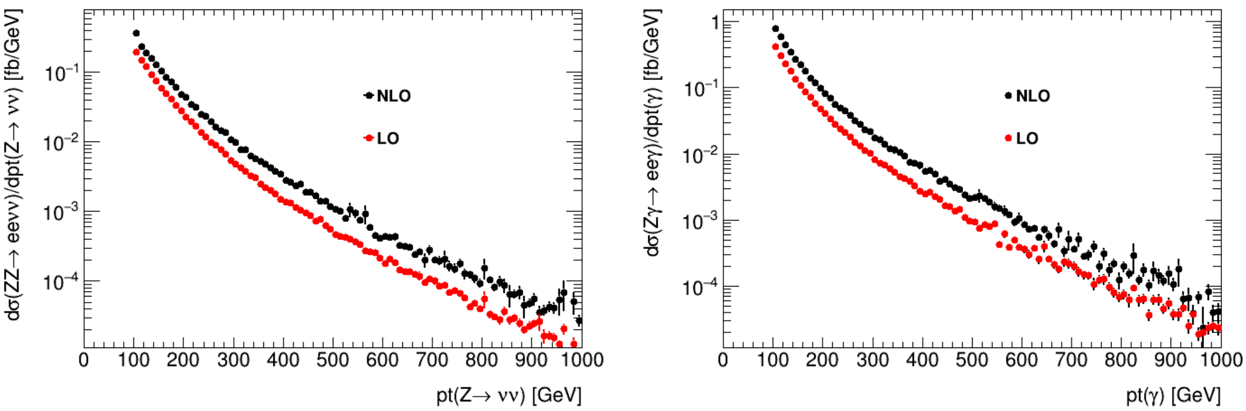

(a) (b)

Figure 4.1: NLO and LO cross sections of $ZZ \to ee\nu\nu$ (left) and $Z\gamma \to ee\gamma$ (right) processes with the cuts as in Table 1. The vertical axis is in $\log_{10}$ scale. The leptonically decaying Z boson decays to an e^+e^- pair. There is no flavor constraint on the neutrinos.

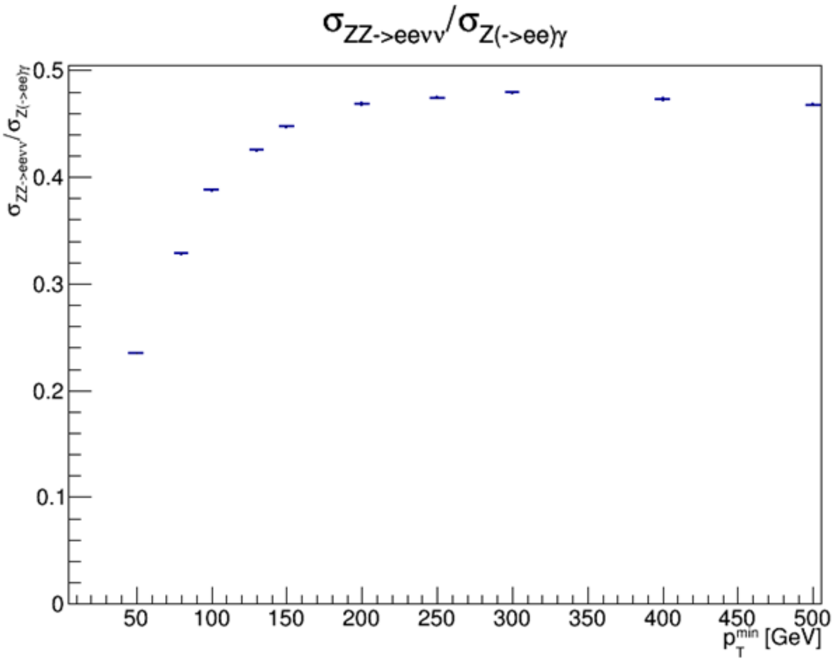

Figure 4.2: The transfer factor R as a function of p_T, taken as a ratio of plots 4.1a and 4.1b. The leptonically decaying Z boson decays to an e^+e^- pair.

The ratio $R = \sigma(ZZ \to ee\nu\nu)/\sigma(Z\gamma \to ee\gamma)$ is shown in Figure 4.2. The R value is observed to increase from ≈ 0.24 at 50 GeV to ≈ 0.47 at high p_T, where it is constant. When the branching ratio of Z boson decaying selectively to e^+e^-, or to $\nu\nu$, is accounted for as shown in Equation 4.1, the resulting ratio $R(p_T)$ is shown in Figure 4.3, which shows the ratio of $\sigma(ZZ)$ to $\sigma(Z\gamma)$, i.e. if the Z bosons do not decay further. The value of R is observed to increase from ≈ 0.61 at 50 GeV to ≈ 1.2 at high p_T, in reasonable agreement with the simple approximate calculation presented in Section 2 of $R \approx 1.28$.

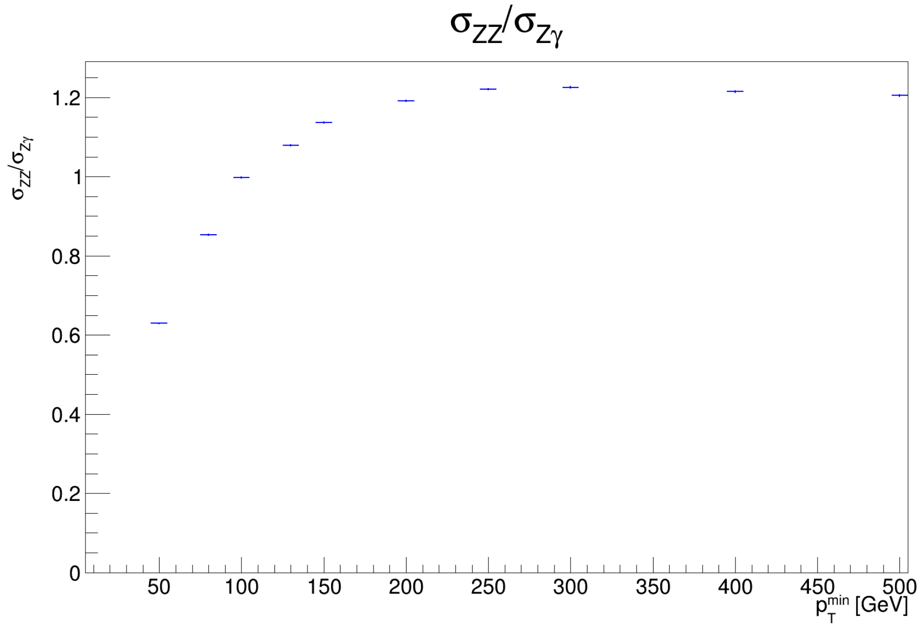

Figure 4.3: The transfer factor R as a function of p_T, adjusted for the $Z \to ee$ and $Z \to \nu\nu$ branching ratios. This shows the $R = \sigma(ZZ)/\sigma(Z\gamma)$, where the Z bosons do not decay.

Gluon-gluon processes contribute to 8.6% of the total cross section for the ZZ process and 2.5% of the $Z + \gamma$ process. Figure 4.4 shows the transfer factor R obtained from the gg process, as well as R from the $q\bar{q}$ and qg processes.

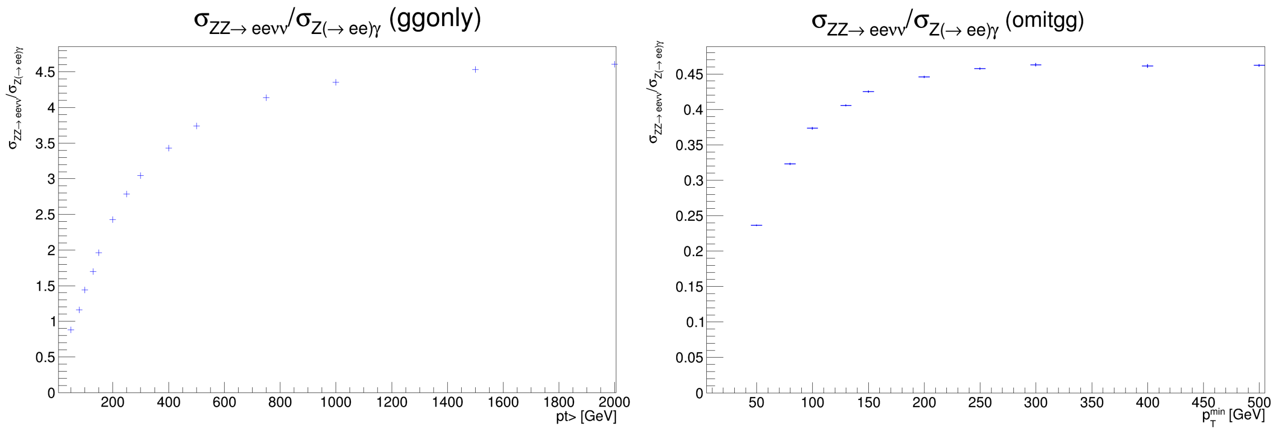

(a) (b)

Figure 4.4: $R(p_T)$ from the contributing gg processes (a), and qg and $q\bar{q}$ processes together (b). The Z bosons decay further to e^+e^- for the leptonic Z boson, or $\nu\nu$ for the invisibly decaying Z boson.

The R_{gg} distribution is observed to approach an asymptotic value at a much higher $p_T = 1.5$ TeV. The shape and scale of the R_{gg} distribution (Figure 4.4a) remain to be understood, as they differ from Figure 4.2.

4.3.1 Effect of Lepton Cuts

To check the effects of lepton cuts on the ratio, samples with the same parameters as those in Table 4.1 are generated. However, we relax the cuts on leptons. Both the leading and subleading lepton should have $p_T > 5$ GeV, and $\eta < 10$. In the lower p_T regions, the cross section falls by nearly half in both processes. The ratio is affected by up to 15% as seen in Figure 4.5, and therefore for all following studies the lepton cuts are applied as they emulate the experimental cuts needed in the analysis.

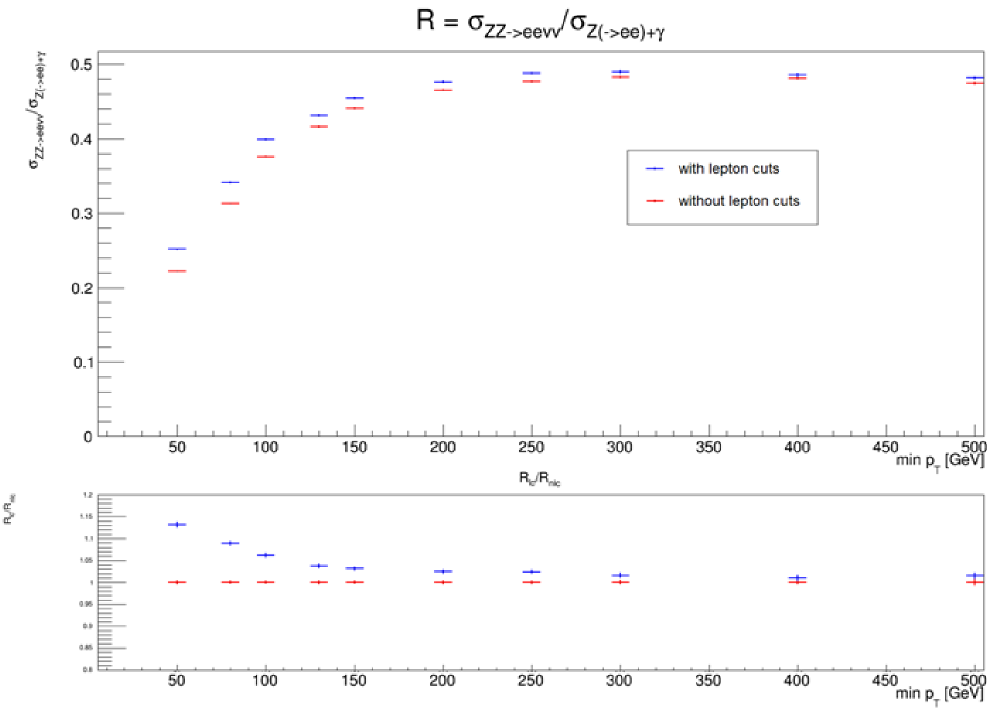

Figure 4.5: Comparison of reference the R distribution to the R distribution without lepton cuts

4.3.2 Uncertainty from Scale Variation

In higher order QCD calculations, perturbative corrections may be added to the vertices or propagators in a Feynman diagram. Physically, these corrections occur at very small time scales. These loop integrals that correspond to these corrections diverge.
The higher the order, the more difficult the calculation is. It is possible to introduce an arbitrary cut-off scale μ such that up to a given order, the effect of these corrections can be absorbed into the strong coupling constant $\alpha_s(\mu)$.
Two kinds of divergences are encountered: infrared divergences, and ultraviolet divergences. Infrared divergences occur for an on-shell internal propagator, and ultraviolet divergences are logarithmic divergences that occur as the integration variable approaches ∞. They correspond to physics at long and short distances[1], respectively. The infrared divergences are addressed by the inclusion of the factorization scale μ_F, while the ultraviolet divergences are addressed by the inclusion of the renormalization scale μ_R. These parameters are arbitrary, and are set by hand. These are then varied between $\frac{1}{2}\mu < \mu < 2\mu$ to obtain an indication of the dependence of the matrix element on the scales, and thus, the uncertainty around the chosen scale.

To address scale uncertainties in this study, the prescription used in [5] is followed. The central scale, μ_0 is chosen to be *something* for both $ZZ \to ll\nu\nu$ and $Z\gamma \to ll\gamma$ samples, and seven-point variations are applied, i.e.

$$\frac{\mu_i}{\mu_0} = (1,1), (1,2), (2,1), (2,2), (0.5,1), (1,0.5), (0.5,0.5) \tag{4.2}$$

where $i = 0, ..., 6$. The central cross section value is taken to be the mean of the maximum and minimum cross sections resulting from this variation, and the uncertainty to be the half the difference

[1]Long distances are those where soft interactions take place, away from the hard parton-parton interaction. Short distances are those where the hard parton parton interactions occur.

between the same.

$$\sigma^{(V)}_{NLO} = \frac{1}{2}\left[\sigma^{(V,max)}_{NLO} + \sigma^{(V,min)}_{NLO}\right] \tag{4.3}$$

$$\delta\sigma^{(V)}_{NLO} = \frac{1}{2}\left[\sigma^{(V,max)}_{NLO} - \sigma^{(V,min)}_{NLO}\right] \tag{4.4}$$

where

$$\begin{aligned} \sigma^{(V,max)}_{NLO} &= max\left\{\sigma^{(V)}_{NLO}(p_T(V),\mu_i)|0 \leq i \leq 6\right\} \\ \sigma^{(V,min)}_{NLO} &= min\left\{\sigma^{(V)}_{NLO}(p_T(V),\mu_i)|0 \leq i \leq 6\right\} \end{aligned} \tag{4.5}$$

and $V = Z \to \nu\nu$ for $ZZ \to ll\nu\nu$, or $V = \gamma$ for $Z\gamma \to ll\gamma$. This uncertainty is propagated to R.

To estimate the degree of correlation between the processes, the process dependent part of the cross sections may be used. Since the study is conducted at NLO, the highest available term in the perturbative expansion is considered to define a K-factor.

$$\Delta K^{(V)}_{NLO} = \sigma^{(V)}_{NLO}(p_T)/\sigma^{(V)}_{LO}(p_T) \tag{4.6}$$

To estimate the unknown process dependent correlation effects, the difference between the QCD K-factors of the $ZZ \to ll\nu\nu$ and $Z\gamma \to ll\gamma$ processes is taken.

$$\delta^{(2)}\sigma_{NLO} = \Delta K^{(\gamma)}_{NLO}(p_T) - K^{(Z)}_{NLO}(p_T) \tag{4.7}$$

4.3.3 Uncertainty from PDF variation

Parton Distribution Functions (PDFs) characterize the fraction of proton momentum carried by partons as probability distributions. PDF sets are collections of PDFs that model parton momenta as accurately as possible. The PDF set used for reference is the `CT14`[6] PDF set. The uncertainty on the PDFs is studied by using the 30 variations provided by the `PDF4LHC15` set[7], constructed from the combination of `CT14,MMHT14`[8] and `NNPDF3.0`[9] PDF sets. These sets are provided by LHAPDF6[10]. `PDF4LHC15` provides a set of variations that include those determined by different groups (MSTW, CTEQ and NNPDF). The set used here is `PDF4LHC15_nlo_30`, consisting of 30 members. While the most accurate uncertainties are given by `PDF4LHC15_nlo_100` set, `PDF4LHC15_nlo_30` is used here for a faster, reasonably accurate estimate of the uncertainties.

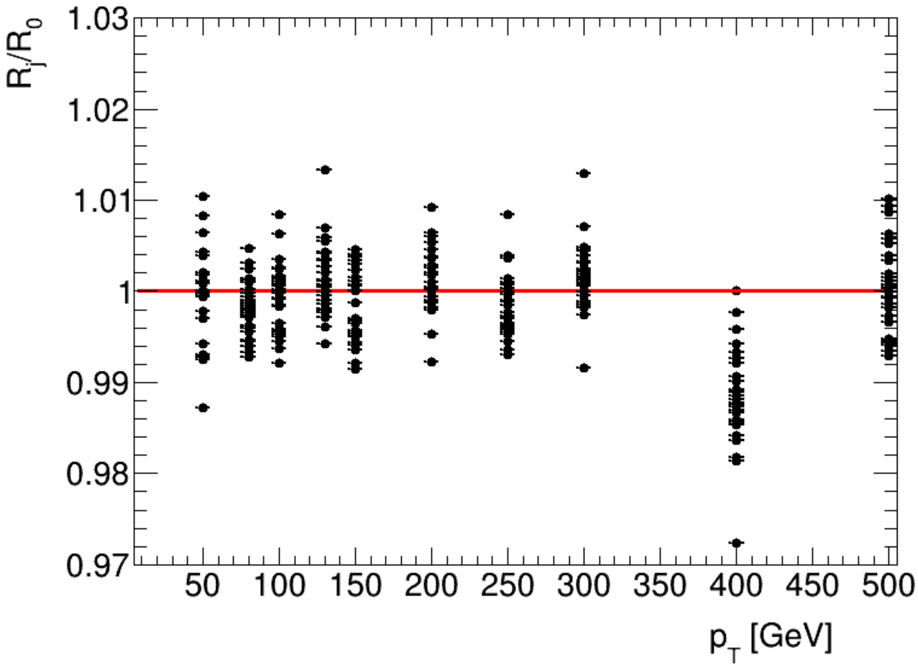

Figure 4.6: The relative ratio R_i/R_0, of the transfer factor $R = \sigma(ZZ)/\sigma(Z\gamma)$ calculated using PDF sets 1-30, with respect to set 0 which is taken as the central value.

Fig.4.6 shows the comparison of the ratio $R(p_T)$ from the 30 member sets of `PDF4LHC15_nlo_30`. To measure the uncertainty due to these 30 sets, analogous to Equation 20 in Ref [7], Equation 4.8 is used:

$$\delta^{PDF} R = \sqrt{\sum_{k=1}^{N_{mem}} (R^{(k)} - R^{(0)})^2} \tag{4.8}$$

where N_{mem} is the number of member sets in the group, in this case, 30. The R distribution obtained from the `PDF4LHC15_nlo_30` set is compared to the reference distributions from `CT14`, as shown in Figure 4.7:

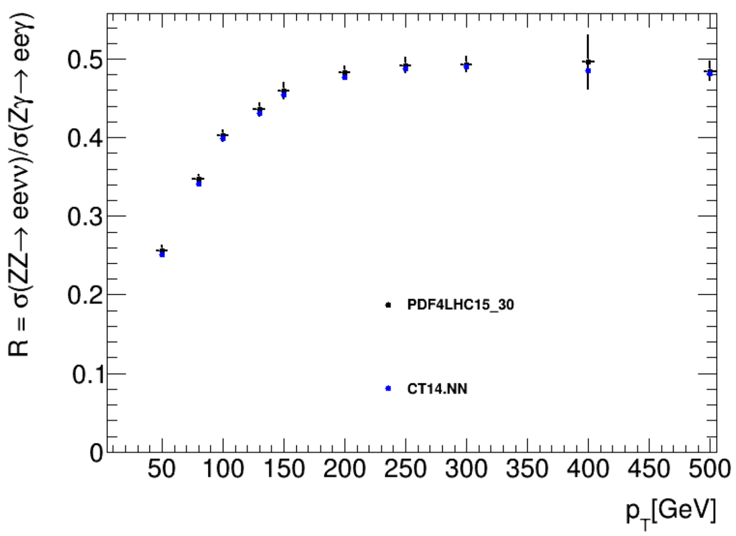

Figure 4.7: The ratio $R(p_T)$ calculated using the PDF sets in `PDF4LHC15_nlo_30` with combined uncertainties as given by Equation 4.8 (blue), compared to the reference constructed from the PDF set `CT14` (red).

Figure 4.7 shows a comparison between the central value of the sets in `PDF4LHC15_nlo_30` with the combined uncertainties, and the reference PDF set `CT14`. The combined uncertainty around $R \approx 0.40$ is $\pm 2.00\%$ at 100 GeV. The R distributions drawn from the two PDF sets agree to within the uncertainty bounds.

4.3.4 Uncertainty from Photon Fragmentation

The $Z\gamma \to ll\gamma$ process may contain photons that arise from the hadron showers. It is therefore important to isolate the prompt photon from hadronic activity. This reduces unwanted background from pion decays, or fragmentation processes.

Experimentally, photon isolation is implemented with the following cuts:

$$\sum_{\in R_0} E_T(\text{had}) < \epsilon_h p_T^{\gamma} \qquad \text{or} \qquad \sum_{\in R_0} E_T(\text{had}) < E_T^{max} \tag{4.9}$$

limiting the transverse hadronic energy $E_T(had)$ in a cone of size $R_0 = \sqrt{\Delta\eta^2 + \Delta\phi^2}$ around the photon, to some fraction of the photon p_T, or some fixed small cut-off.

The smooth cone isolation method of Frixione [11] is an alternative isolation procedure, which simplifies calculations by avoiding fragmentation contribuitions. The following isolation prescription is applied to the photon:

$$\sum_{R_{j\gamma} \in R_0} E_T(\text{had}) < \epsilon_h p_T^{\gamma} \left(\frac{1 - \cos R_{j\gamma}}{1 - \cos R_0} \right)^n . \tag{4.10}$$

where $R_{j\gamma}$ is the separation of the photon and the j^{th} hadron. This requirement constrains the sum of hadronic energy inside a cone of radius $R_{j\gamma}$, for all separations $R_{j\gamma}$ less than a chosen cone size R_0. This prescription allows soft radiation inside the photon cone, but collinear singularities are removed. The smooth cone isolation is infrared finite, thus fragmentation contributions do not need to be included.
The relative isolation, given by Equation 4.3.4 is used in experimental analyses, while smooth isolation is difficult to implement experimentally. However, comparing both methods gives us an estimate of the uncertainty due to the modelling of photon fragmentation.

In this analysis, R_0 is chosen to be 0.4 to agree with the experimental definition. The central value is chosen to be from the sample using smooth cone isolation (Frixione) with $\epsilon_h = 0.075$ and $n = 1$. These parameters are varied within a reasonable range to assess the uncertainty as shown in Figure 4.8.

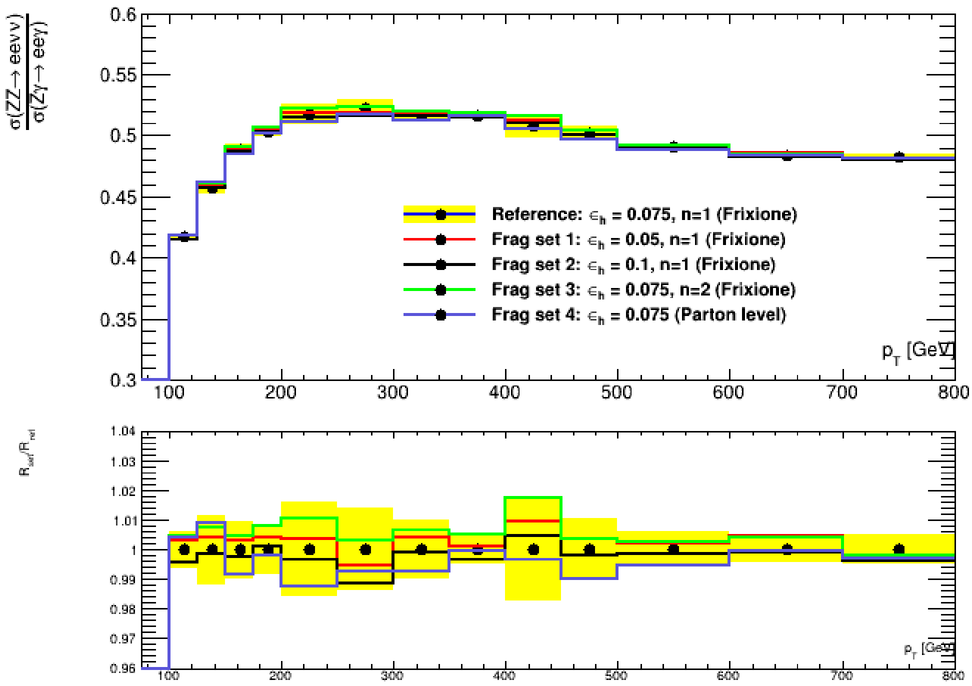

Figure 4.8: R distribution as a function of p_T, showing the uncertainty due to variation of photon isolation parameters ϵ_h and n in the smooth cone isolation procedure (Frixione), and ϵ_h in the photon isolation procedure. The lower panel shows the relative deviation of the varied sets from the central value, as well as the uncertainty band.

The uncertainty is calculated from the four sets listed in Figure 4.8:

$$\begin{aligned} \delta R_i &= |R_i - R_{ref}| \qquad\qquad i \in (1,2,3,4) \\ \delta R &= \sqrt{\max_{i=1,2,3}(\delta R_i)^2 + (\delta R_4)^2} \end{aligned} \tag{4.11}$$

as the effects assessed by changing the isolation definition in set 4, and varying the parameters in sets 1-3 are different.

The uncertainty is $< 2\%$ over the whole range, which has been extended up till 800 GeV.

Bibliography

[1] *Search for an invisibly decaying Higgs boson or dark matter candidates produced in association with a Z boson in pp collisions at $\sqrt{s}$ = 13 TeV with the ATLAS detector*
ATLAS Collaboration
arXiv:1708.09624

[2] *Using γ+ jets to calibrate the Standard Model $Z(\rightarrow \nu\nu)$+ jets background to new processes at the LHC*
S. Ask, M. A. Parker, T. Sandoval, M. E. Shea, W. J. Stirling
Cavendish Laboratory, University of Cambridge, CB3 0HE, UK; 2011
[arXiv:1107.2803]

[3] *2017 Review of Particle Physics - Particle Listings*
C. Patrignani *et al.* (Particle Data Group)
Chin. Phys. C, 40, 100001 (2016)

[4] *Monte Carlo for FeMtobarn processes (MCFM) v8.0 User Manual*
John Campbell, Keith Ellis, Walter Giele, Ciaran Williams
https://mcfm.fnal.gov/

[5] *Precise predictions for V +jets dark matter backgrounds*
J.M. Lindert, S. Pozzorini, et al.
arXiv:1705.04664

[6] *New parton distribution functions from a global analysis of quantum chromodynamics*
Sayipjamal Dulat, Tie Jiun Hou, Jun Gao, Marco Guzzi, Joey Huston, P. Nadolsky, Jon Pumplin, Carl Schmidt, Daniel Stump, C. P. Yuan
arXiv:1506.07443

[7] *PDF4LHC recommendations for LHC Run II*
[arXiv:1510.03865]

[8] *Parton distributions in the LHC era: MMHT 2014 PDFs*
L. A. Harland-Lang, A. D. Martin, P. Motylinski, R. S. Thorne
arXiv:1412.3989

[9] *Parton distributions for the LHC Run II*
The NNPDF Collaboration: Richard D. Ball, Valerio Bertone, Stefano Carrazza, Christopher S. Deans, Luigi Del Debbio, Stefano Forte, Alberto Guffanti, Nathan P. Hartland, Jose I. Latorre, Juan Rojo, Maria Ubiali
arXiv:1410.8849

[10] *LHAPDF6: parton density access in the LHC precision era*
Andy Buckley, James Ferrando, Stephen Lloyd, Karl Nordstrom, Ben Page, Martin Ruefenacht, Marek Schoenherr, Graeme Watt
arXiv:1412.7420

[11] *Isolated photons in perturbative QCD*
S. Frixione
Phys. Lett.B429(1998)369–374, hep-ph/9801442